Effect of nano-CaCo3 on hydration of cement containing supplementary cementitious materials

NRCC-53922

Sato, T.; Beaudoin, J.J.

October 2010

A version of this document is published in / Une version de ce document se trouve dans:
Advances in Cement Research, 23, (1), pp. 1-29, October 2010

Title: Effect of Nano-$CaCO_3$ on Hydration of Cement Containing Supplementary Cementitious Materials

Authors: Taijiro Sato (Lead Author) and James J. Beaudoin

Affiliation: Institute for Research in Construction, National Research Council Canada

Email Address: Taijiro.Sato@nrc-cnrc.gc.ca

Telephone: (613) 993-0089

Fax: (613) 954-5984

Postal Address: 1200 Montreal Rd., Building M-20, Ottawa, ON, K1A 0R6, Canada

Number of Words: 3444

Number of Figures: 12

Number of Tables: 1

Abstract

The efficacy of the addition of nano-$CaCO_3$ in accelerating the hydration of ordinary Portland cement (OPC) delayed by the presence of high volumes of supplementary cementitious materials including fly ash and slag was investigated. The conduction calorimetry indicated that the early hydration of OPC was significantly accelerated by the addition of the nano-$CaCO_3$ and the higher the amount of $CaCO_3$ addition, the greater was the accelerating effect. The thermogravimetric analysis results showed that the amounts of added $CaCO_3$ became slightly lower as the hydration took place; however any new reaction products were not detected by the X-ray diffractometry analysis. The engineering properties including microhardness and modulus of elasticity, in the early stage of the hydration were remarkably improved by the addition of nano-$CaCO_3$. It was suggested that the seeding effect of the nano-$CaCO_3$ particles and the nucleation of C-S-H caused the enhanced strength development.

Introduction

The use of supplementary cementitious materials (SCMs) such as fly ash and slag as partial replacements of ordinary Portland cement (OPC) in concrete is widely known in the cement industry. It reduces not only the amount of industrial by-products going to landfills, but also the natural resources used in the manufacture of OPC and the associated CO_2 emissions, which accounts for about 7% of the global CO_2 emissions (Worrell et al., 2001). Some of the SCMs also improve the long-term engineering properties of concrete, through a pozzolanic or hydraulic property of SCMs. One of the major drawbacks of concrete containing high volumes of SCMs, however, is the resulting delayed setting and slower initial strength development (Mehta and Gjørv, 1982). This issue becomes even more critical in cold weather (Bouzoubaâ and Fournier, 2003). The compensation of the delayed setting and slower initial strength development is essential as the use of high volumes of SCMs becomes popular.

The use of ground limestone ($CaCO_3$) as a replacement of OPC in concrete is widely practiced (Neville, 1995). The behavior of $CaCO_3$ in the hydration of OPC has also been intensively studied (Barker and Cory, 1991; Ingram and Daugherty, 1991; Kakali et al., 2000; Matschei et al., 2007). The results from a number of studies have indicated the positive effects of the $CaCO_3$ addition on the hydration of cement paste and strength development of hardened concrete, especially its accelerating effect on the rate of hydration. A study on the accelerating effect of the finely ground $CaCO_3$ addition on the hydration of C_3S was conducted (Ramachandran and Zhang, 1986). It was concluded that the hydration of C_3S was significantly accelerated and the higher the $CaCO_3$ addition, the

greater was the accelerating effect. The accelerating effect of the addition of the finely ground limestone on the hydration of OPC was also observed (Péra et al., 1999).

The results of a study designed to determine the efficacy of the nano-$CaCO_3$ in accelerating the hydration of OPC delayed by the presence of high volumes of fly ash or slag are presented in this paper. A comparison was made with that of the micro-$CaCO_3$ by determining the rate of heat development and mechanical properties. The interaction of the nano-$CaCO_3$ with OPC was also examined by the thermogravimetric analysis and X-ray diffractometry.

Experimental

Materials

Ordinary Portland cement (OPC), Class "F" fly ash and ground granulated blast-furnace slag were supplied by Lafarge, Shaw Resources and the Standard Slag Cement Co., respectively. Reagent grade micro-$CaCO_3$ and nano-$CaCO_3$ were supplied by Anachemia Canada Inc and READE, respectively. High purity water, supplied by Anachemia Canada Inc., was used as mixing water.

Sample Specifications and Experimental Techniques

The sample specifications for each experimental technique are shown in Table 1. The percentages of the $CaCO_3$ content in Table 1 were based on the binder mass (OPC for Series 1 and OPC + fly ash or slag for Series 2 and 3). The percentages of the fly ash content for Series 2 and the slag content for Series 3 were also based on the binder mass. A water/binder ratio (w/b) of 0.5 was used. A high-speed mechanical shaker was used for

10 seconds to blend the unhydrated OPC with micro- or nano-$CaCO_3$ before mixing with water for a better dispersion. The mechanical shaker was also used for the OPC Control, so that all the samples, with or without $CaCO_3$, were subjected to the 10-second shaking to keep them consistent in terms of a possible effect of the shaking on the samples. This blending process was used for the samples of all experimental techniques except for raw materials.

The scanning electron microscope (SEM) images were obtained using an Hitachi S4800 field emission gun scanning electron microscope with the accelerating voltage and the emission current at 1.2 keV and 7 μA, respectively. The nitrogen BET surface area of both micro- and nano-$CaCO_3$ was determined using a Quantachrome Nova 2200e surface area analyzer. The conduction calorimetry was performed using the Thermometric TAM Air Isothermal Calorimeter, 3114/3236 to determine the rate of heat development. The rate of heat development was calculated in joules per binder mass per hour. Thermogravimetric analysis (TGA) was conducted, using a TA Instruments, Q600, to calculate the amount of $CaCO_3$ in the samples. The temperature was ramped from room temperature to 1050°C at 10°C/min with a 100 ml/min nitrogen gas flow. The X-ray diffractometry (XRD) measurements were collected, using a Scintag, XDS 2000 with CuK_α radiation and a graphite monochrometer. Continuous scans were performed at every 0.02° per second from 5° to 60° (2θ). The results were analysed using JADE software (Materials Data Inc.). The helium pycnometer, the Quantachrome Corporation, Stereopycnometer, was used to determine the porosity of the samples. A hydrated specimen was sliced into a circular plate, about 31.5 mm in diameter and 1.0 mm in thickness. It was weighed and its

dimensions were determined prior to the testing to calculate the bulk volume of the specimen. For TGA, XRD and helium pycnometry, the samples were immersed in isopropanol for 2 hours to stop hydration at a desired hydration period and dried under vacuum for 18 hours. The microhardness determination was performed using the DURIMET, Small-hardness Tester to study the surface characteristics and mechanical behaviour of the samples. A circular plate specimen was prepared in the same manner as the helium pycnometry. The microhardness was determined by the average of 49 indentations on the surface of the circular plate specimen under a static loading. The modulus of elasticity was determined using an instrument designed and fabricated at National Research Council Institute for Research in Construction. A circular plate specimen prepared in the same manner as the helium pycnometry was supported at 3 points and the deflection at the center point was recorded with various loadings. TGA, XRD, helium pycnometry, microhardness and modulus of elasticity measurements were performed at 1-, 3-, 7-, 14- and 28-day hydration with the addition of 10-hour hydration period for TGA and XRD.

Results and Discussion

The scanning electron microscope (SEM) images, for each $CaCO_3$ type are shown in Fig. 1 (a) and (b), with magnifications of ×5,000 and ×50,000, respectively. The particle size, observed by the SEM, of the micro-$CaCO_3$ was approximately 5 to 20 μm, whereas that of nano-$CaCO_3$ was about 50 to 120 nm. The nitrogen BET surface area results for the micro- and nano-$CaCO_3$ were 0.35 and 20.50 m^2/g, respectively. The following part of this

section consists of two parts. In the first part, the effect of each micro- and nano- $CaCO_3$ addition on the hydration of OPC will be discussed (Series 1 in Table 1). No SCMs were therefore used. In the second part, the effect of each micro- and nano-$CaCO_3$ addition on the hydration of OPC – fly ash binder and OPC – slag binder will be discussed (Series 2 and 3 in Table 1).

Effect of the micro- and nano-$CaCO_3$ additions on the hydration of OPC

The conduction calorimetry results for the OPC Control and OPC with the additions of 10% and 20% of micro-$CaCO_3$ and nano-$CaCO_3$ for w/b of 0.50 (Series 1 in Table 1) are shown in Fig. 2. The rate of heat development of OPC was slightly accelerated by the additions of 10% and 20% micro-$CaCO_3$ compared to the OPC Control. A similar slight acceleration of hydration of OPC by the addition of micro-$CaCO_3$ was previously observed (Péra et al., 1999; Lothenbach et al. 2008). It was concluded that the additional surface provided by the addition of micro-$CaCO_3$ for the nucleation and growth of the hydration products was the reason for the observed slight acceleration. The rate of heat development of the OPC was significantly accelerated by the additions of both 10% and 20% nano-$CaCO_3$ compared to the OPC Control and it was clearly indicated that the higher the amount of nano-$CaCO_3$ addition, the greater was the accelerating effect. It is well-known that the conduction calorimetry curve of OPC has a small shoulder right after the main peak of hydration as shown in Fig. 2. It has been suggested that this shoulder is associated with the renewed formation of ettringite (Taylor, 1997). With the addition of the 20% nano-$CaCO_3$, this shoulder was not only significantly accelerated but also

enhanced as shown in the figure. It indicates that the formation of ettringite and/or similar compounds may have been enhanced by the addition of nano-$CaCO_3$.

The TGA was conducted to determine the amount of $CaCO_3$, both the amount of $CaCO_3$ originally in the OPC and the amount of $CaCO_3$ separately added, in the samples hydrated for 0 hours (unhydrated), 10 hours, 1 day and 3 days. The results are shown in Fig. 3. The 10-hour hydration period was included to investigate the effect of the enhanced heat development shown in Fig. 2 on the amount of $CaCO_3$ in the sample. The percentages of $CaCO_3$ were normalised to the mass of OPC of the samples prior to the test. It should be noted that the TGA analysis gave 98.6% of $CaCO_3$ for testing the 99.0% pure control micro-$CaCO_3$ and 94.8% for the 98.0%-pure control nano-$CaCO_3$. The TGA result of the control nano-$CaCO_3$ showed a mass loss of about 2.5% before 600°C. A further study is needed to determine whether this mass loss is because of the decomposition of nano-$CaCO_3$ or possibly because some nano-particles may have been blown away from the sample cup by the 100 ml/min nitrogen gas flow. However, the determination of the amount of $CaCO_3$ in the OPC samples shown in Fig. 3 depends on the decomposition peak that occurs after 600°C. As a result, the amount of nano-$CaCO_3$ shown in Fig. 3 was corrected for the mass loss before 600°C. There was about 2.3% of $CaCO_3$ in the unhydrated OPC Control. Thus the unhydrated OPC with the additions of micro- and nano-$CaCO_3$ had values about 2.3% higher than the added amount of $CaCO_3$. A decrease of the amount of $CaCO_3$ in the OPC with the additions of 10% and 20% nano-$CaCO_3$ after 10-hour hydration was relatively higher than that with the additions of 10% and 20% micro-$CaCO_3$ as shown in Fig. 3. It may relate to the presence of the shoulder on the rate

of heat development curve. This was enhanced by the addition of the nano-$CaCO_3$ and occurred just before the 10-hour hydration, as indicated in Fig. 2. It has been reported that the $CaCO_3$ in OPC may chemically react with tricalcium aluminate, C_3A to form calcium carboaluminate hydrates with or without the presence of gypsum (Ingram et al., 1990; Ramachandran, 1988). The chemical reaction of C_3A with $CaCO_3$ produces both high- and low- carbonate forms of calcium aluminate hydrate, respectively, $3CaO{\cdot}Al_2O_3{\cdot}3CaCO_3{\cdot}32H_2O$ and $3CaO{\cdot}Al_2O_3{\cdot}CaCO_3{\cdot}11H_2O$. This chemical reaction is very similar to that of C_3A with $CaSO_4{\cdot}2H_2O$ (gypsum) that produces both high- (ettringite) and low- sulphate forms of calcium aluminate hydrate (Carleson and Berman, 1960; Klemm and Adams, 1990). The decrease of the amount of $CaCO_3$ in the first 10 hours may be due to the consumption of $CaCO_3$ by the chemical reaction with C_3A. The decrease of the amount of $CaCO_3$ with the addition of nano-$CaCO_3$ in the first 10 hours was higher than that with the micro-$CaCO_3$. The amount of $CaCO_3$ continued to decrease as the hydration took place and it was higher with the nano-$CaCO_3$.

The XRD was also conducted for Series 1 shown in Table 1. Figure 4 shows the XRD results of the OPC Control and OPC with the additions of 20% micro- and nano-$CaCO_3$ at 1-day hydration. The peaks of ettringite were observed in all samples, however, the peak intensities were lower with both the micro- and nano-$CaCO_3$ than those with the OPC Control, indicating that the amounts of ettringite formed were lower with the micro- and nano-$CaCO_3$. The peaks for calcium carboaluminate hydrates, the other possible hydration products due to the addition of $CaCO_3$, were very small even with the intensive scan of the XRD. A study using pure compounds, such as a reaction between C_3A and nano-$CaCO_3$,

may be needed to investigate possible chemical reactions of nano-$CaCO_3$ during the hydration of OPC.

Effect of the micro- and nano-$CaCO_3$ additions on the hydration of OPC containing high volumes of SCMs

The conduction calorimetry results for the samples in Series 2 and Series 3 in Table 1 are shown in Figs. 5 and 6, respectively. In Fig. 5, the hydration of OPC – fly ash binder was significantly delayed compared to that of the OPC Control, owing to the lower cement content in the sample. The rate of heat development of the OPC – fly ash binder was slightly accelerated by the additions of both 10% and 20% micro-$CaCO_3$. The slight acceleration by the addition of the micro-$CaCO_3$ was also observed with the OPC Control as shown in Fig. 2. When the nano-$CaCO_3$ was added, the rate of heat development was significantly accelerated and the higher the $CaCO_3$ addition, the greater was the accelerating effect. The hydration of OPC – slag binder was not delayed as much as OPC – fly ash binder, as shown in Fig. 6. A slight acceleration was observed with the additions of both 10% and 20% micro-$CaCO_3$. Again, the rate of heat development was significantly accelerated with the addition of nano-$CaCO_3$, and the higher the $CaCO_3$ addition, the greater was the accelerating effect.

The microhardness results for the samples in Series 2 in Table 1, hydrated up to 3 days and 28 days are shown in Fig. 7 (a) and (b), respectively. The early strength development of the OPC – fly ash binder shown in Fig. 7 (a) was significantly delayed. The microhardness of the OPC – fly ash binder was very similar to that with the micro-$CaCO_3$,

which was expected from the conduction calorimetry results. The microhardness of OPC – fly ash binder, however, became considerably higher with the addition of the nano-$CaCO_3$. Those results were consistent with the observation from the conduction calorimetry curves shown in Fig. 5, where the rate of heat development was delayed by the presence of high volumes of fly ash and accelerated by the nano-$CaCO_3$.

The microhardness results for the samples in Series 3 in Table 1, hydrated up to 3 days and 28 days are shown in Fig. 8 (a) and (b), respectively. The microhardness of the OPC – slag binder were significantly increased by the additions of 10% and 20% nano-$CaCO_3$. The rate of heat development of OPC was not delayed as much as the OPC – fly ash binder as shown in Fig. 6. However the microhardness of OPC – slag binder was as low as OPC – fly ash binder. In the case of slag, enhanced strength development was also observed with the micro-$CaCO_3$; this was not the case with fly ash. Figures 7 (b) and 8 (b) both indicate that the strength development enhanced by the addition of nano-$CaCO_3$, continued up to 28-day hydration. It is generally known that the long-term strength development is likely to be unaffected even if the early hydration is accelerated by the admixture (Transportation Research Board, 1990). This was not the case with the addition of nano-$CaCO_3$. The strength development in the early stages of hydration accelerated by the addition of $CaCO_3$ continued to improve up to 28-day hydration.

It was previously indicated that a small portion of the added $CaCO_3$ may be interacting in the hydration process. However, the hydration products directly interacted with $CaCO_3$ may not be responsible for the improvement of strength development. In Fig. 2, not only

the small shoulder of the calorimetry curve, but also the whole main peak of the calorimetry curve was enhanced and accelerated by the addition of nano-$CaCO_3$. This main peak is primarily attributed to the hydration of C_3S. This is critical to strength development and it is clear that the significant strength development shown in Figure 6 was a result of the accelerated hydration of C_3S. The study on the effect of the finely ground limestone addition on the hydration of C_3S noted that the reaction products formed between the hydrating C_3S and the added $CaCO_3$ could not be identified, as they were present in only small amounts (Ramachandran, 1988). This indicates that there was likely something else responsible for accelerating the hydration and the significant strength development. One possible explanation is the seeding effect of the nano-$CaCO_3$ particles on the nucleation of C-S-H. The nucleation of C-S-H was accelerated by the presence of the well-crystalline nano-$CaCO_3$ particles on the surface of the OPC grains. The effect of two calcareous fillers, ground limestone and reagent grade $CaCO_3$ on the compressive strength of OPC was studied and it was argued that the calcareous fillers acted as nucleation sites responsible for the acceleration effect on the early strength development (Soroka and Stern, 1976). However, a further study is needed to investigate the seeding effect of the nano-$CaCO_3$ particles for the nucleation of C-S-H. The seeding effect of the nano-$CaCO_3$ for the nucleation of C-S-H should be distinguished from the effect for the slight acceleration of OPC by the addition of micro-$CaCO_3$. As mentioned earlier, the slight acceleration of OPC by the addition of micro-$CaCO_3$ has been explained by the additional surface provided by the addition of micro-$CaCO_3$ for the nucleation and growth of the hydration products (Péra et al., 1999; Lothenbach et al., 2008). The surface of the

micro-$CaCO_3$ was provided for OPC to form more C-S-H. In the case of the nano-$CaCO_3$, each nano-$CaCO_3$ particle may promote formation of C-S-H on the OPC grains.

The modulus of elasticity results for the samples in Series 2 in Table 1, hydrated up to 3 days and 28 days are shown in Fig. 9 (a) and (b). The results for the samples in Series 3 in Table 1 hydrated up to 3 days and 28 days are shown in Fig. 10 (a) and (b). The modulus of elasticity results were very similar to those of microhardness. The early development of modulus of elasticity in the presence of fly ash or slag was significantly improved by the addition of nano-$CaCO_3$. In the case of modulus of elasticity, the influence of the micro-$CaCO_3$ was relatively greater than in the case of the microhardness.

The porosity determinations were performed for the samples in Series 2 and 3 in Table 1 using the helium pycnometer. The results were plotted against microhardness as shown in Figs. 11 and 12, respectively. For each set of the results, the regression analysis was performed. Figure 11 indicates that the OPC Control had the highest values of microhardness and OPC – fly ash binder the lowest. The microhardness with the additions of $CaCO_3$ were in the following order: OPC – fly ash binder with 20% nano-$CaCO_3$ > 10% nano-$CaCO_3$ > 10% micro-$CaCO_3$ and > 20% micro-$CaCO_3$. Figure 12 also indicates that the OPC Control was much higher than that for the OPC – slag binder. The microhardness with the additions of $CaCO_3$ was in the following order: OPC – slag binder with 20% nano-$CaCO_3$ >10% nano-$CaCO_3$ > 20% micro-$CaCO_3$ and > 10% micro-$CaCO_3$. It should be noted that the regression curve with the addition of the 20% nano-$CaCO_3$ intersects with the OPC Control at a porosity of 41%. This implies that the microhardness

of the OPC Control was lower than that of OPC – slag binder with the addition of the 20% nano-$CaCO_3$ when the porosity was lower than 41%, and higher when the porosity was greater than 41%. The microhardness – porosity results provide a valid comparison for the cement systems studied. The validity of the comparison is however limited to the porosity range of the experimental data. The physical meaning of microhardness values outside the porosity range of the experimental data is complex. Dense crystalline products, for example, can have microhardness values lower or higher than the OPC Control depending on the porosity range. The effect of grain boundaries and defects at low porosities can contribute to the non-linear behaviour in the microhardness – porosity plots.

Conclusions

The efficacy of the addition of nano-$CaCO_3$ in accelerating the hydration of OPC delayed by the presence of high volumes of SCMs was investigated. The conduction calorimetry indicated that the early hydration of the OPC was significantly accelerated by the addition of the nano-$CaCO_3$ and the higher the amount of $CaCO_3$ addition, the greater was the accelerating effect. The TGA results showed that the amounts of added $CaCO_3$ became slightly lower as the hydration took place; however any new reaction products were not detected by the XRD analysis. The engineering properties including microhardness and modulus of elasticity, in the early stage of the hydration were remarkably improved by the addition of the nano-$CaCO_3$. It was suggested that the seeding effect of the nano-$CaCO_3$ particles and the nucleation of C-S-H caused the enhanced strength development. Further study is needed to confirm this.

References

Barker A. and Cory H., The Early Hydration of Limestone-filled Cements. In: N. Swamy, Editor, *Blended Cements in Construction*, Elsevier, London, 1991, 107–124

Bouzoubaâ N. and Fournier B. Current Situation of SCMs in Canada *CANMET Report MTL 2003-4 (TR)*, Natural Resources Canada, Ottawa, April 2003.

Carleson E.T. and Berman H.A., Some Observations on the Calcium Aluminate Carbonate Hydrates, *Journal of Research of the National Bureau of Standards – A. Physics and Chemistry*, 64A, 4, 1960, 333-341

Ingram K.D. and Daugherty K.E., A Review of Limestone Additions to Portland Cement and Concrete, *Cement and Concrete Composites*, 1991, 13, 3, 165-170

Ingram K., Poslusny M., Daugherty K. and Rowe W. Carboaluminate Reactions as Influenced by Limestone Additions, In: P. Klieger and R.D. Hooton, Editors, *Carbonate Additions to Cement*, STP 1064, ASTM, Philadelphia, 1990, 14–23.

Kakali G., Tsivilis S., Aggeli E. and Bati M., Hydration Products of C_3A, C_3S and Portland Cement in the Presence of $CaCO_3$, *Cement and Concrete Research*, 2000, 30, 7, 1073-1077

Klemm W.A. and Adams L.D., An Investigation of the Formation of Carboaluminates in Carbonate Additions to Cement, In: P. Klieger and R.D. Hooton, Editors, *Carbonate Additions to Cement*, STP 1064, ASTM, Philadelphia, 1990, 60-72

Lothenbach B., Le Saout G., Gallucci E. and Scrivener K., Influence of Limestone on the Hydration of Portland Cements, *Cement and Concrete Research*, 2008, 38(6), 848-860

Matschei T., Lothenbach B. and Glasser F.P., The Role of Calcium Carbonate in Cement Hydration, *Cement and Concrete Research*, 2007, 37, 4, 551-558

Mehta P.K. and Gjørv O.E. Properties of Portland Cement Concrete Containing Fly Ash and Condensed Silica-fume, *Cement and Concrete Research*, 1982, 12, 5, 587-595

Neville A.M. *Properties of Concrete (4th edition)* Prentice Hall, Harlow, UK, 1995.

Péra J., Husson S. and Guilhot B., Influence of Finely Ground Limestone on Cement Hydration, *Cement and Concrete Composites*, 1999, 21(2), 99-105

Ramachandran V.S. Thermal Analysis of Cement Components Hydrated in the Presence of Calcium Carbonate, *Thermochimica Acta*, 127, 1988, 385-394

Ramachandran V.S. and Zhang C., Influence of $CaCO_3$ on Hydration and Microstructural Characteristics of Tricalcium Silicate, *II Cemento*, 1986, 83(3), 129-152

Soroka I. and Stern N., Calcareous Fillers and the Compressive Strength of Portland Cement, *Cement and Concrete Research*, 1976, 6(7), 367-376

Taylor H.F.W., *Cement Chemistry (2nd edition)* Thomas Telford, London, 1997.

Transportation Research Board, Admixtures and Ground Slag for Concrete, *Transportation Research Circular no. 365 (December)*, 1990, Washington: Transportation Research Board, National Research Council

Worrell E., Price L., Hendricks C., Meida L.O., Carbon Dioxide Emissions from the Global Cement Industry, Annual Review of Energy and Environment, 2001, 26, 303-329

Table 1: Sample specifications for each experimental technique

		SEM	BET Surface Area	Conduction Calorimetry	TGA	X-ray Diffraction	Helium Pycnometry	Microhardness	Modulus of Elasticity
Raw Materials	Micro-$CaCO_3$	✓	✓	-	-	-	-	-	
	Nano-$CaCO_3$	✓	✓	-	-	-	-	-	
Series 1 (w/b 0.50)	OPC [100%] Control	-	-	✓	✓	✓	-	-	-
	OPC [100%] + Micro-$CaCO_3${10%}*	-	-	✓	✓	✓	✓	✓	✓
	OPC [100%] + Nano-$CaCO_3${10%}	-	-	✓	✓	✓	-	-	-
	OPC [100%] + Micro-$CaCO_3${20%}	-	-	✓	✓	✓	-	-	-
	OPC [100%] + Nano-$CaCO_3${20%}	-	-	✓	✓	✓	-	-	-
Series 2 (w/b 0.50)	OPC [50%] + Fly Ash [50%]	-	-	✓	-	✓	✓	✓	✓
	OPC [50%] + Fly Ash [50%] + Micro-$CaCO_3${10%}	-	-	✓	-	✓	✓	✓	✓
	OPC [50%] + Fly Ash [50%] + Nano-$CaCO_3${10%}	-	-	✓	-	✓	✓	✓	✓
	OPC [50%] + Fly Ash [50%] + Micro-$CaCO_3${20%}	-	-	✓	-	✓	✓	✓	✓
	OPC [50%] + Fly Ash [50%] + Nano-$CaCO_3${10%}	-	-	✓	-	✓	✓	✓	✓
Series 3 (w/b 0.50)	OPC [50%] + Slag [50%]	-	-	✓	-	✓	✓	✓	✓
	OPC [50%] + Slag [50%] + Micro-$CaCO_3${10%}	-	-	✓	-	✓	✓	✓	✓
	OPC [50%] + Slag [50%] + Nano-$CaCO_3${10%}	-	-	✓	-	✓	✓	✓	✓
	OPC [50%] + Slag [50%] + Micro-$CaCO_3${20%}	-	-	✓	-	✓	✓	✓	✓
	OPC [50%] + Slag [50%] + Nano-$CaCO_3${20%}	-	-	✓	-	✓	✓	✓	✓

* The $CaCO_3$ contents are expressed as a percentage of the total binder content (i.e. OPC, OPC + Fly Ash or OPC + Slag)

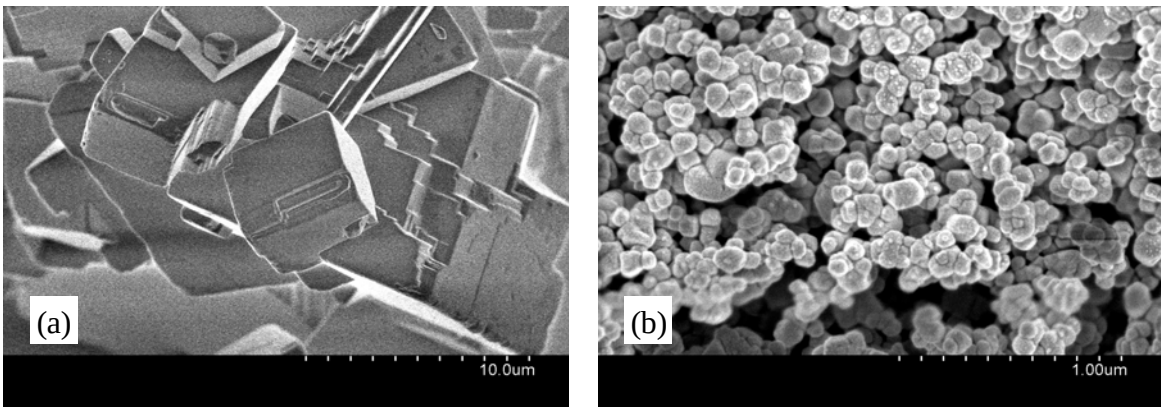

Fig. 1: SEM images of (a) micro-$CaCO_3$ and (b) nano-$CaCO_3$ with magnifications of ×5,000 and ×50,000, respectively

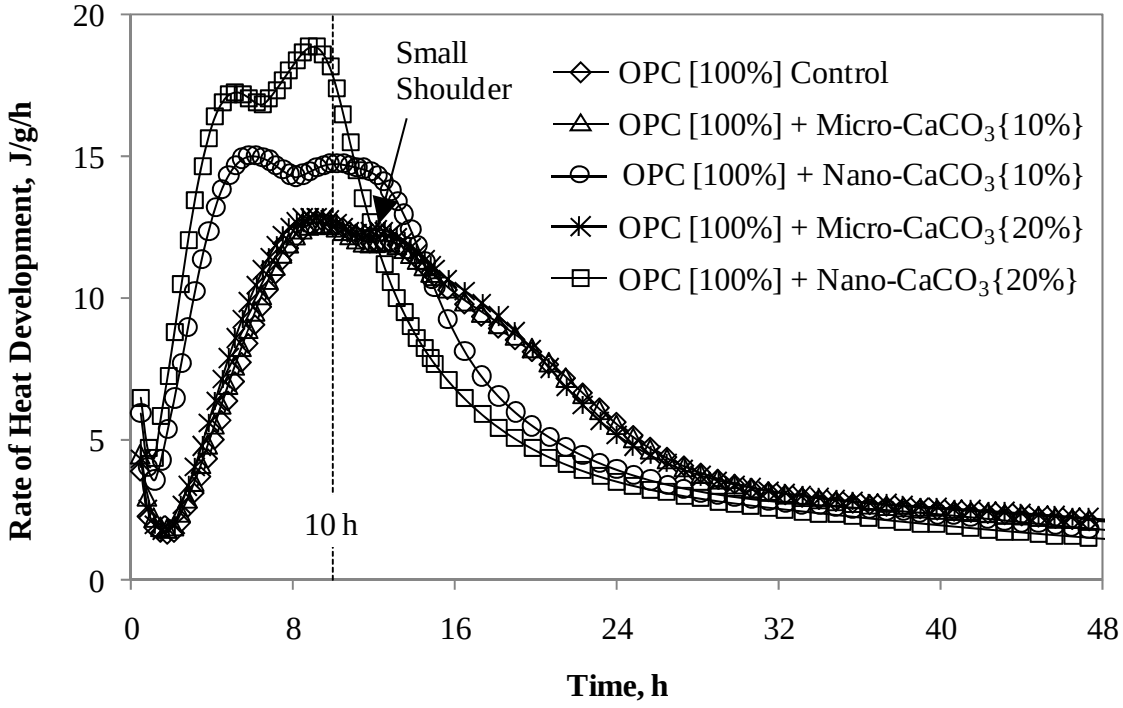

Fig. 2: Conduction calorimetry results for OPC Control and OPC with the additions of micro- and nano-$CaCO_3$ for w/b of 0.50

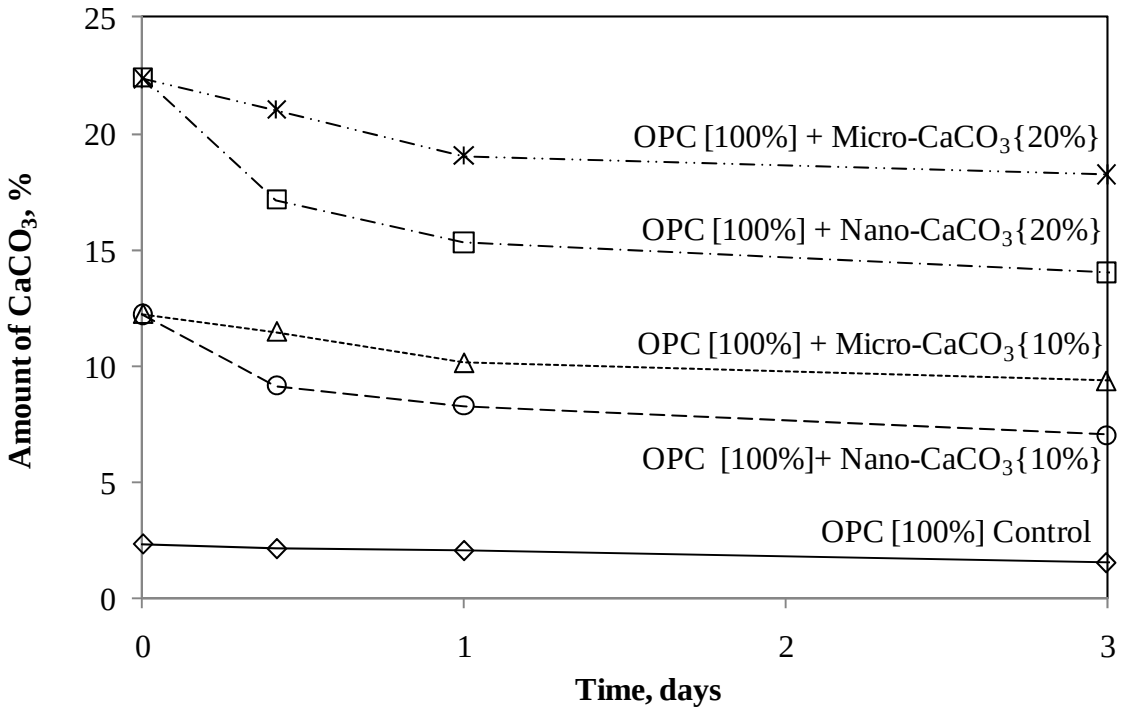

Fig. 3: The amounts of $CaCO_3$, determined by TGA, for the OPC Control and OPC with the additions of micro- and nano-$CaCO_3$ for w/b 0.50 at 0, 10-hour, 1-day and 3-day hydration

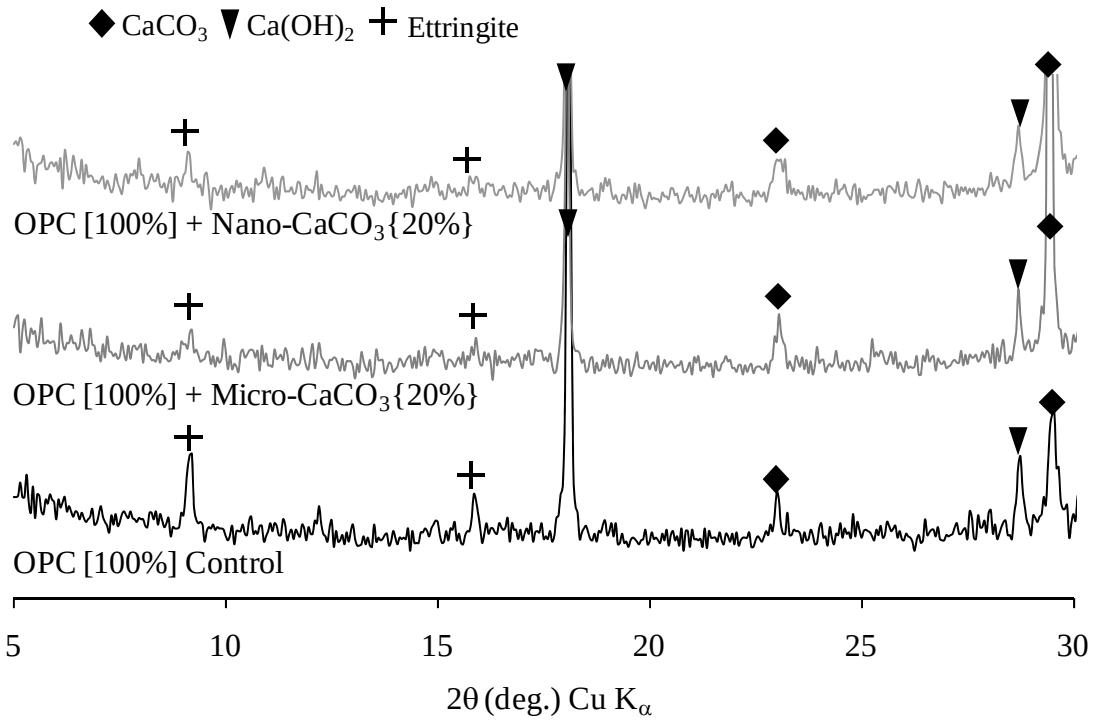

Fig. 4: The XRD results of the OPC Control and OPC with the 20% additions of micro- and nano-$CaCO_3$ for w/b 0.50 at 1-day hydration

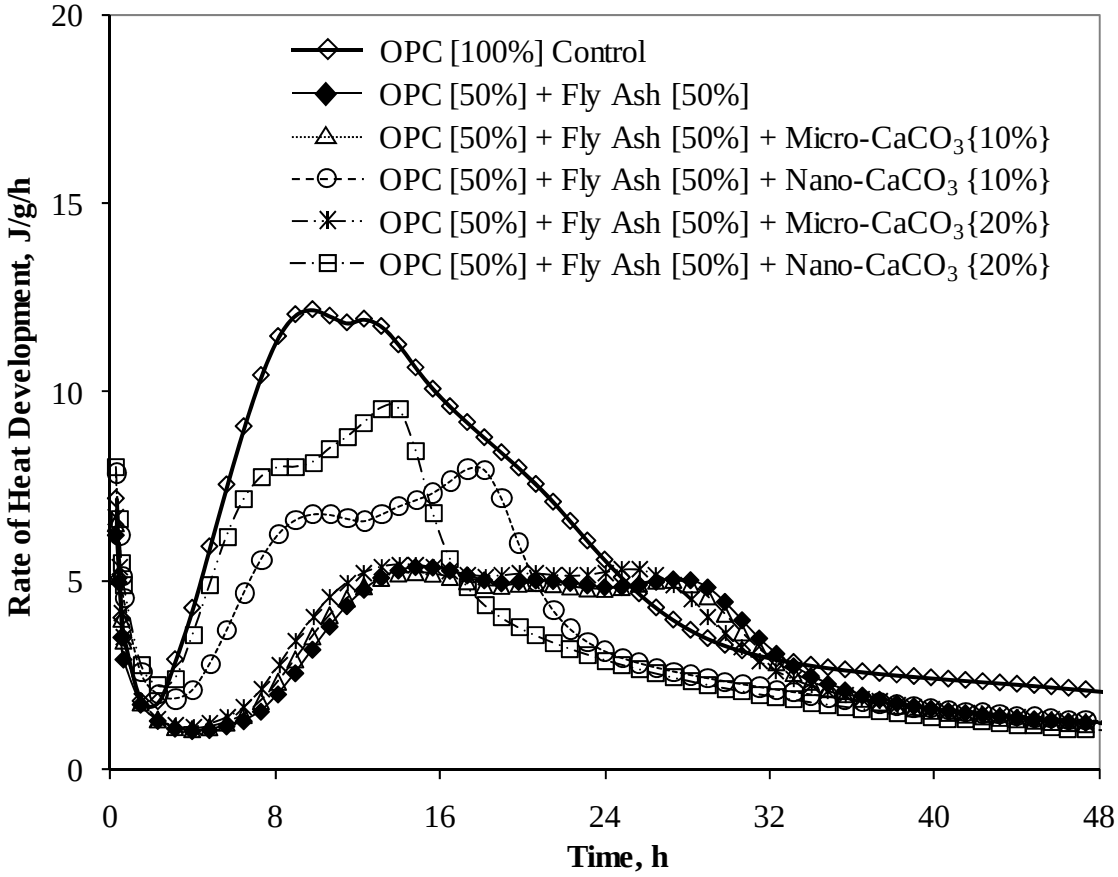

Fig. 5: Conduction calorimetry results for OPC Control, OPC – fly ash binder and OPC – fly ash binder with the additions of micro- and nano-$CaCO_3$ for w/b 0.50

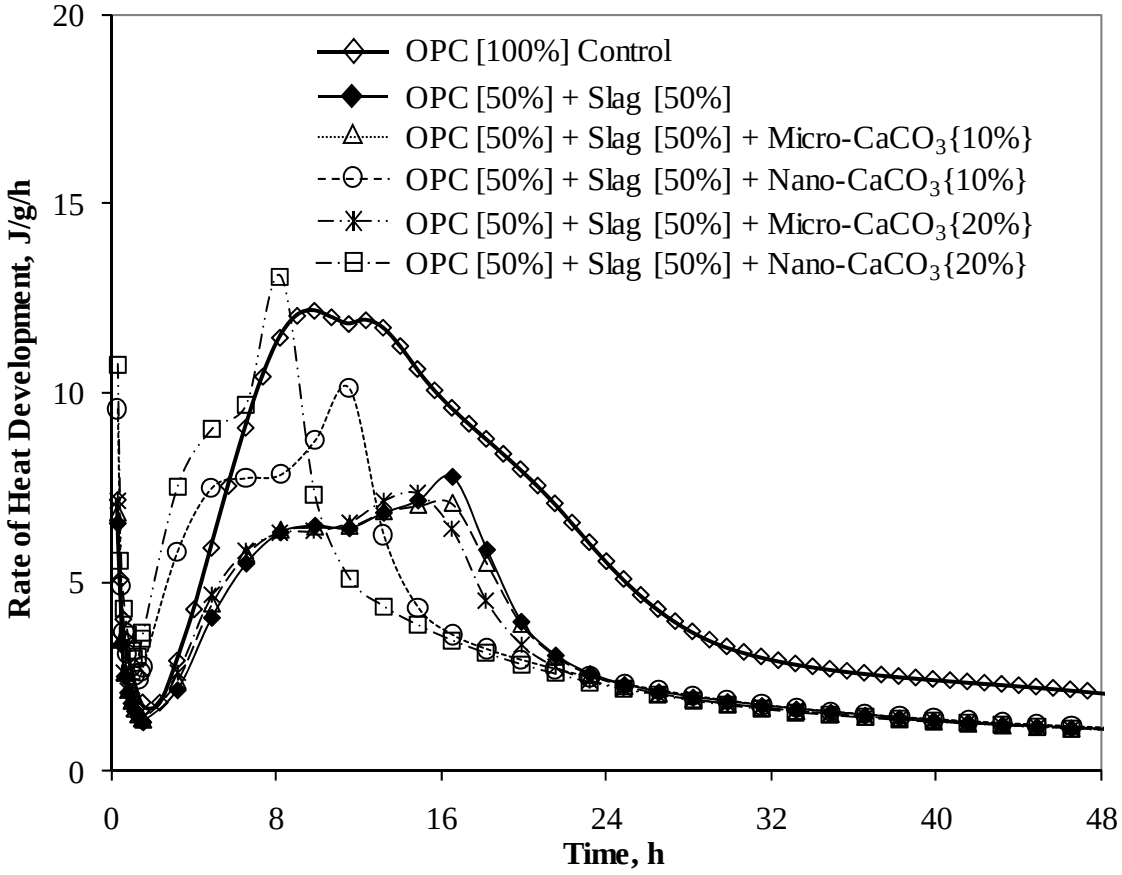

Fig. 6: Conduction calorimetry results for OPC Control, OPC – slag binder and OPC – slag binder with the additions of micro- and nano-$CaCO_3$ for w/b 0.50

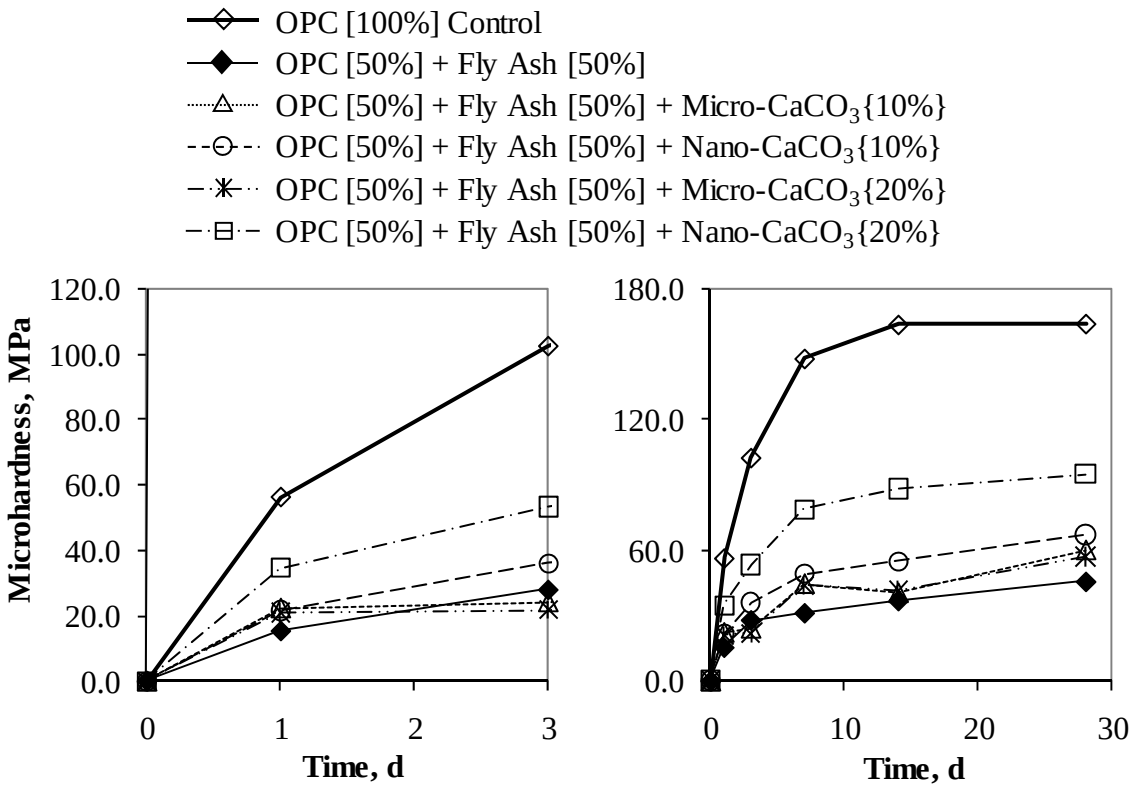

Fig. 7: Microhardness results for OPC Control, OPC – fly ash binder and OPC – fly ash binder with the additions of micro- and nano-$CaCO_3$ for w/b 0.50 for (a) 3-day and (b) 28-day hydration

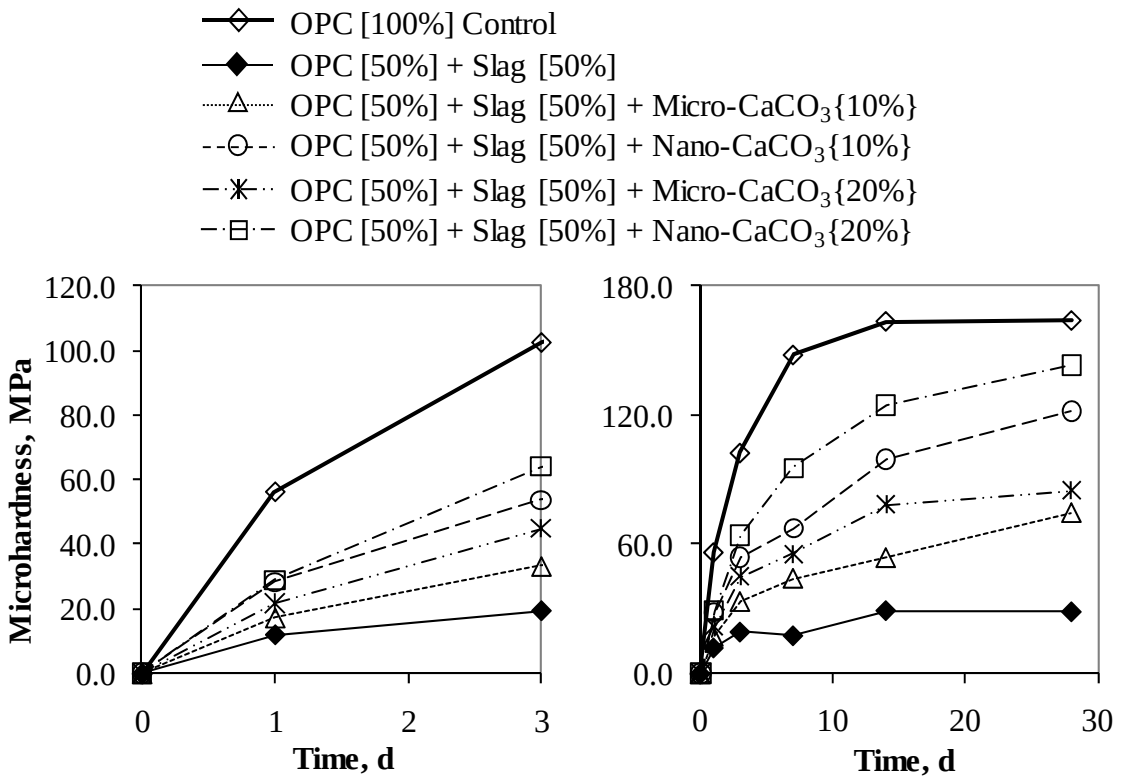

Fig. 8: Microhardness results for OPC Control, OPC – slag binder and OPC – slag binder with the additions of micro- and nano-$CaCO_3$ for w/b 0.50 for (a) 3-day and (b) 28-day hydration

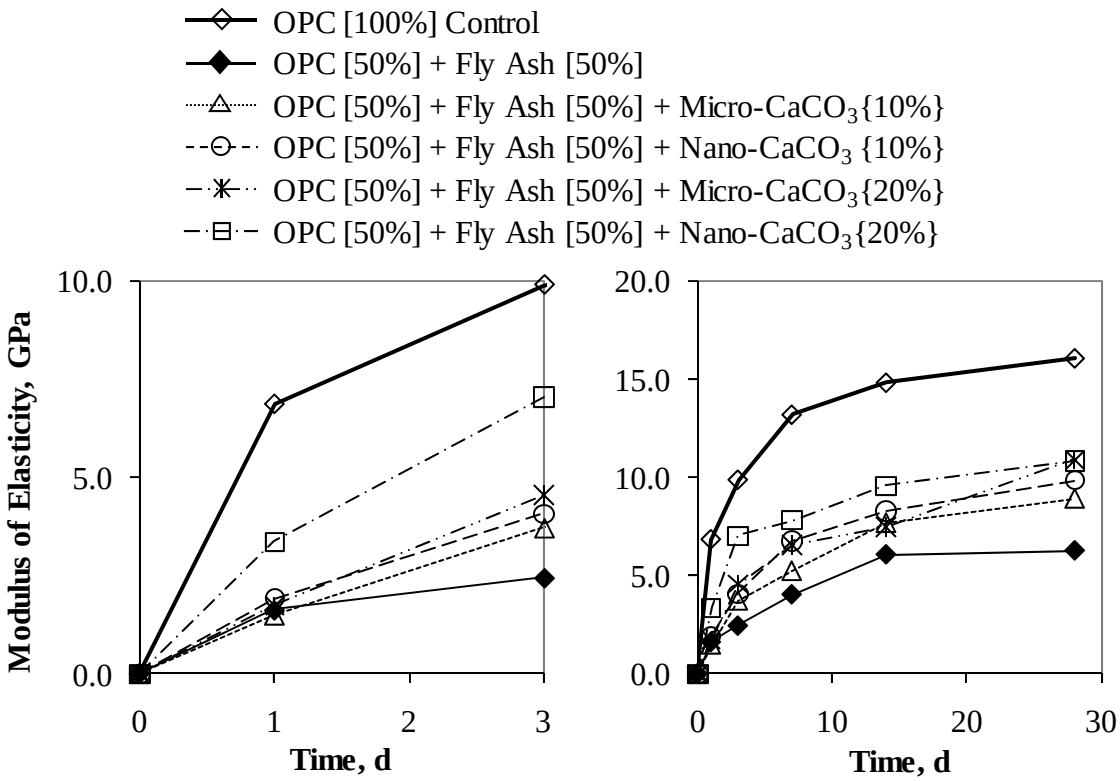

Fig. 9: Modulus of elasticity results for OPC Control, OPC – fly ash binder and OPC – fly ash binder with the additions of micro- and nano-$CaCO_3$ for w/b 0.50 for (a) 3-day and (b) 28-day hydration

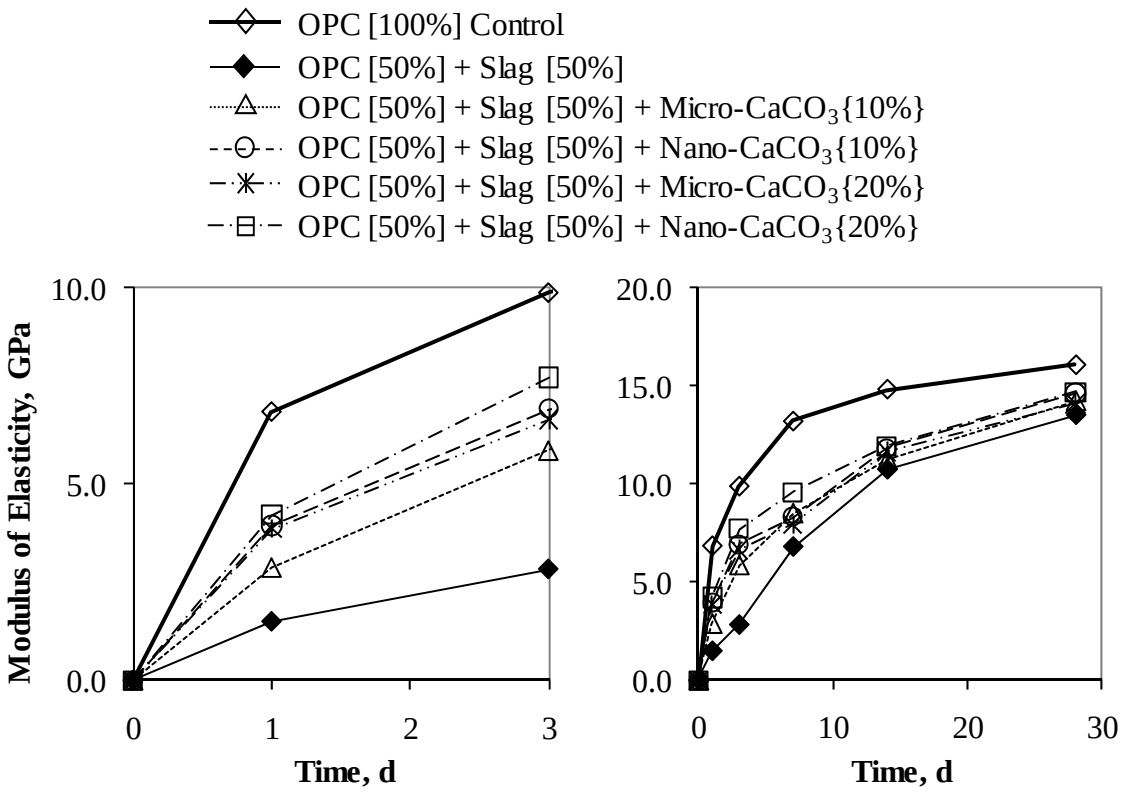

Fig. 10: Modulus of elasticity results for OPC Control, OPC – slag binder and OPC – slag binder with the additions of micro- and nano-$CaCO_3$ for w/b 0.50 for (a) 3-day and (b) 28-day hydration

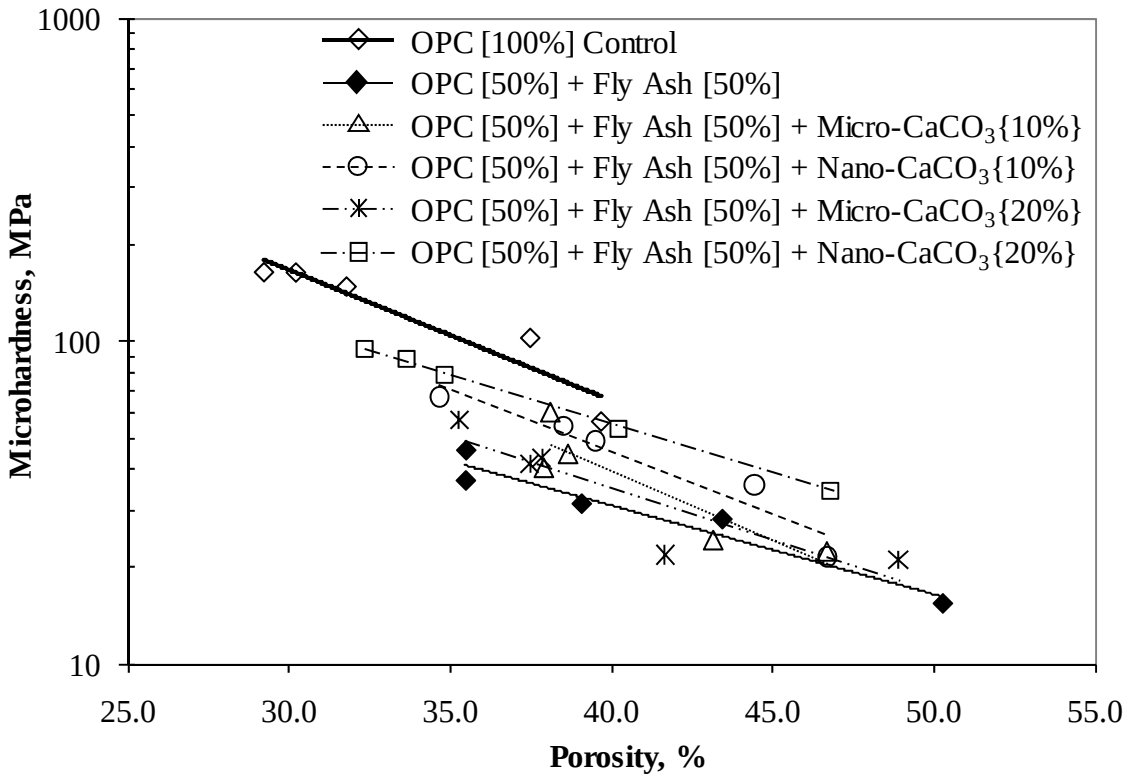

Fig. 11: The logarithms of microhardness values versus porosity for OPC Control, OPC – fly ash binder and OPC – fly ash binder with the additions of micro- and nano-$CaCO_3$

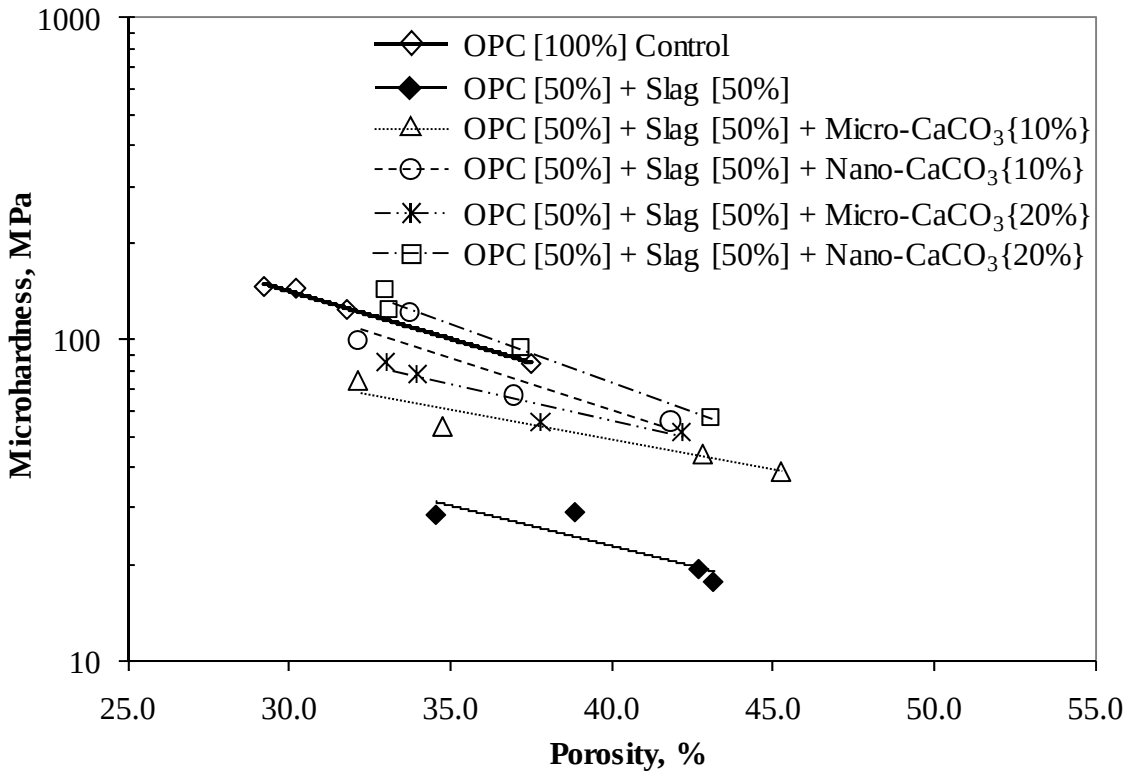

Fig. 12: The logarithms of microhardness values versus porosity for OPC Control, OPC – slag binder and OPC – slag binder with the additions of micro- and nano-$CaCO_3$